

2004

Estimation of Drag Coefficient in James River Estuary Using Tidal Velocity Data from a Vessel-Towed ADCP

Chunyan Li

Arnoldo Valle-Levinson
Old Dominion University

Larry P. Atkinson
Old Dominion University, latkinso@odu.edu

Kuo Chuin Wong

Kamazima M. M. Lwiza

Follow this and additional works at: https://digitalcommons.odu.edu/ccpo_pubs

 Part of the [Oceanography Commons](#)

Repository Citation

Li, Chunyan; Valle-Levinson, Arnoldo; Atkinson, Larry P.; Wong, Kuo Chuin; and Lwiza, Kamazima M. M., "Estimation of Drag Coefficient in James River Estuary Using Tidal Velocity Data from a Vessel-Towed ADCP" (2004). *CCPO Publications*. 98.
https://digitalcommons.odu.edu/ccpo_pubs/98

Original Publication Citation

Li, C. Y., Valle-Levinson, A., Atkinson, L. P., Wong, K. C., & Lwiza, K. M. M. (2004). Estimation of drag coefficient in James River Estuary using tidal velocity data from a vessel-towed ADCP. *Journal of Geophysical Research-Oceans*, 109(C03034), [1-11]. doi: 10.1029/2003jc001991

Estimation of drag coefficient in James River Estuary using tidal velocity data from a vessel-towed ADCP

Chunyan Li,¹ Arnoldo Valle-Levinson,² Larry P. Atkinson,² Kuo Chuin Wong,³ and Kamazima M. M. Lwiza⁴

Received 2 June 2003; revised 1 November 2003; accepted 19 January 2004; published 20 March 2004.

[1] A phase-matching method is introduced to calculate the bottom drag coefficient in tidal channels with significant lateral variation of depth. The method is based on the fact that the bottom friction in a tidal channel causes tidal velocity to have a phase difference across the channel. The calculation involves a few steps. First, the observed horizontal velocity components are analyzed to obtain the amplitude and phase of the velocity at the major tidal frequency. The phase of the longitudinal velocity is then fitted to a relationship derived from the linearized momentum balance. The drag coefficient is then calculated. This method is applicable to narrow (approximately a few kilometers wide) tidal channels without strong stratification and where the cross-channel variation of surface elevation is negligible compared to tidal amplitude. This analytic approach is easy to implement when appropriate observational data are available. It allows a spatial variation of the drag coefficient, and the resolution is only limited by that of the observations. The method is validated by identical twin experiments and applied to tidal velocity data, obtained in the James River Estuary, using an acoustic Doppler current profiler during spring tides and neap tides in October–November 1996. The obtained bottom drag coefficient ranged from 1.2×10^{-3} to 6.9×10^{-3} at different positions along two cross-channel transects each 4 km long and 2 to 14 m deep. The maximum drag coefficient is found in the shallowest water near the banks of the estuary, while the minimum values occur between 9 and 12 m in the center of the channel. The friction of the lateral boundary may have contributed to the apparent increase of the bottom friction on the banks. The transverse mean values of the drag coefficient ranges between 2.2 and 2.3×10^{-3} for the spring and neap tides, respectively. **INDEX TERMS:** 4594 Oceanography: Physical: Instruments and techniques; 4203 Oceanography: General: Analytical modeling; 4560 Oceanography: Physical: Surface waves and tides (1255); 4568 Oceanography: Physical: Turbulence, diffusion, and mixing processes; **KEYWORDS:** drag coefficient, tides, analytic model

Citation: Li, C., A. Valle-Levinson, L. P. Atkinson, K. C. Wong, and K. M. M. Lwiza (2004), Estimation of drag coefficient in James River Estuary using tidal velocity data from a vessel-towed ADCP, *J. Geophys. Res.*, 109, C03034, doi:10.1029/2003JC001991.

1. Introduction

[2] A depth-averaged hydrodynamic model is often used to study tidal properties in a shallow estuary, where the maximum water depth is on the order of a few tens of meters. In such a model, the intensity of the overall energy dissipation is related to the surface and bottom drag coefficients. For the major tidal frequency component, only the bottom drag coefficient is relevant and the wind stress usually has lower and variable frequencies. The estimation

of the bottom drag coefficient can be accomplished by (1) a simple scaling argument (a straightforward order of magnitude estimate) [Godfrey, 1980], (2) a dimensional analysis using the logarithmic law [Lueck and Lu, 1997], (3) comparisons of results from a highly simplified analytic model to observational data [Wang and Craig, 1993], or (4) full-scale assimilative numerical models, the so-called adjoint variational method [Spitz and Klinck, 1998; Ullman and Wilson, 1998]. A scaling argument is useful when very little information is available. However, this simple method is often not the best choice when there is a large amount of data available which can provide more information than just an order-of-magnitude estimate. Dimensional analysis is applicable to a steady and uniform flow over an immobile flat bed with no boundary. Some studies have suggested that it can be applied to tidal flow problems when the temporal variation of flow is taken into account [Wilkinson, 1986; Friedrichs and Wright, 1997; Kuo et al., 1996]. The comparison of an analytic model with observations, while useful for ideal cases, is difficult to generalize because

¹Skidaway Institute of Oceanography, Savannah, Georgia, USA.

²Center for Coastal Physical Oceanography, Old Dominion University, Norfolk, Virginia, USA.

³College of Marine Studies, University of Delaware, Newark, Delaware, USA.

⁴Marine Sciences Research Center, State University of New York, Stony Brook, New York, USA.

analytic models often require regular geometry of the region. The adjoint variational method has been developed for various long wave problems [Thacker, 1988; Thacker and Long, 1988; Thacker, 1989; Panchang and Richardson, 1993; Ten Brummelhuis et al., 1993; Lardner and Das, 1994; Lardner and Song, 1995] and used by some studies to estimate parameters using field observations in, for example, the Chesapeake Bay [Spitz, 1995] and the Hudson River Estuary [Ullman and Wilson, 1998].

[3] The adjoint variational method requires two numerical models: One is essentially the same as an ordinary numerical model, except that the parameters are to be determined by the model solution, and the other is the adjoint variational model which must be integrated backward in time. The parameters are determined by minimizing a cost function which represents the misfit between the data and the model solution.

[4] A non-adjoint variational numerical method has also been developed [Bang, 1994] to estimate both the horizontal pressure gradient and vertical eddy viscosity by assimilating data of a vertical profile of horizontal tidal velocity obtained at a single station. The bottom drag coefficient is derived after the eddy viscosity and horizontal pressure gradient are calculated.

[5] One alternative to the complex adjoint variational method is using an analytic method by fitting observational data to the momentum equations at the major tidal frequency [Bowden and Fairbairn, 1952; Huntley et al., 1994]. This method does not need a “first guess” or “initial value” but requires an accurate measurement of the pressure gradient. Since the pressure gradient ($\sim 10^{-4}$ – 10^{-5} m/s²) related to tidal motion is proportional to a small difference between two relatively large numbers (the tidal elevations) divided by a close distance, it is not trivial to directly measure the pressure gradient in the field with a good accuracy.

[6] In this paper, we introduce an analytic method, which does not require a direct measurement of the horizontal pressure gradient, to calculate the effective bottom drag coefficient by assimilating semi-diurnal tidal velocity data obtained from an acoustic Doppler current profiler (ADCP) along a transverse transect in a narrow estuary. We call it the Phase-Matching Method. The horizontal pressure gradient can then be obtained after the drag coefficient is estimated. It should be noted that the method presented here uses a drag coefficient defined by the depth-averaged velocity as in numerous applications for practical reasons [e.g., Proudman, 1953; Godfrey, 1980; Parker, 1984; Wang and Craig, 1993; Ullman and Wilson, 1998; Spitz and Klinck, 1998]. This is in contrast to the bottom drag coefficient defined by the vertical profiles of the flow [e.g., Lueck and Lu, 1997]. The two types of drag coefficient are not necessarily equal to each other since they are defined in different momentum equations (one with depth-averaged velocity and the other with the three-dimensional velocity). They should, however, be consistent as far as the overall energy dissipation is concerned. The method is developed in section 2 and applied to the ADCP data from the James River Estuary in section 3. In section 4, we demonstrate with some identical twin experiments using a two-dimensional tidal model that the phase-matching method can correctly recover the bottom drag coefficient in a two-dimensional tidal model. In section 4, we also use the

calculated drag coefficient in the two-dimensional model to calculate the flow field which is compared with the observations. We then summarize the results in section 5.

2. Phase-Matching Method

[7] According to the scaling analysis of Bang [1994], the baroclinic pressure gradient in a typical shallow estuary is about 2 orders of magnitude smaller than the barotropic pressure gradient. As a result, the pressure gradient in shallow water waves tends to be depth-independent in estuaries with typical longitudinal density gradient values. This is true, of course, at the major tidal frequency when only the linear momentum balance is considered. As a first-order approximation, we therefore assume that it is sufficient to include only the barotropic component of the pressure gradient at the major tidal frequency. The nonlinear dynamics including overtides and compound tides [e.g., Parker, 1984, 1991] are neglected. At subtidal frequencies, the baroclinic pressure gradient will be important for most estuaries [e.g., Hansen and Rattray, 1965], a regime that we do not discuss here. The nonlinear effect will complicate the problem substantially to prevent an analytic approach.

[8] The depth-averaged longitudinal momentum equation for an estuary without Coriolis force is [e.g., LeBlond, 1978; Clarke, 1990; Wang and Craig, 1993]:

$$\frac{\partial u}{\partial t} = -g \frac{\partial \zeta}{\partial t} - \frac{\beta}{h} u, \quad (1)$$

where u , ζ , x , t , h , β , and g are the longitudinal velocity, surface elevation, longitudinal coordinate, time, the undisturbed water depth, bottom friction coefficient, and acceleration due to gravity, respectively. By neglecting the Coriolis force in the longitudinal momentum balance, we are limiting our discussion to narrow estuaries or tidal channels in which the transverse velocity v is much smaller than the longitudinal velocity u so that $|fv| \ll |\partial u/\partial t|$. Using the James River as an example, the width is on the order of 4 km and the transverse velocity is on the order of 10 cm/s, about 10% of the longitudinal velocity. The friction coefficient β is defined by [Proudman, 1953; Parker, 1984]

$$\beta = \frac{8C_D U_0}{3\pi}, \quad (2)$$

in which C_D and U_0 are the bottom drag coefficient and the magnitude of the tidal velocity. In general, U_0 is a function of position and is to be determined by observations. Following Bowden and Fairbairn [1952] and Huntley et al. [1994], we consider the semi-diurnal tidal component only. We write

$$u = \text{Re}\{Ue^{i\sigma t}\}, \quad \zeta = \text{Re}\{Ae^{i\sigma t}\}, \quad (3)$$

where σ , i , U , A , ζ , and Re are the angular frequency of the semi-diurnal tide, the unit imaginary number ($\sqrt{-1}$), the complex amplitude of the longitudinal velocity, the complex amplitude of the tide, the semi-diurnal tidal elevation, and a mathematical operator which produces the real part of the complex number inside the braces, respectively.

[9] By substituting equation (3) into equation (1), we obtain the following:

$$U = -\frac{g}{i\sigma + \beta/h} \frac{\partial A}{\partial x}. \quad (4)$$

[10] A direct analysis of equation (4) can provide us with physical insights. For instance, the magnitude of the velocity is $|U| = \alpha h / \sqrt{\sigma^2 h^2 + \beta^2}$, where α is a constant with units of m s^{-2} at a given x . For a typical shallow estuary, the larger h is, the larger $|U|$ will be, although the relationship is not linear, particularly at large h (>20 m). In practice, with known vertical profiles of the velocity, the depth-averaged velocity U can be obtained. However, since the longitudinal pressure gradient ($\partial A/\partial x$) is unknown, the drag coefficient C_D or the friction coefficient β cannot be estimated from the magnitude of equation (4) in general. However, an examination of the phase relationship obtained from equation (4) may provide new insights, and a method can be developed to estimate the unknown drag coefficient. To illustrate this, we note that friction is crucial in determining the characteristics of tide: if β is zero, then both $|U|$ and the phase of U will be independent of h . With friction, both the flood and ebb occur first at shallow water. The phase lag of along channel velocity can be on the order of 1 hour [e.g., *Valle-Levinson et al.*, 1998]. This fact can be seen from the dependence of phase of along-channel velocity on the variation of water depth: $-\tan^{-1}(\sigma h/\beta)$, which gives a larger value for a smaller h ; that is, the phase in shallow water leads that in deep water as demonstrated by a 2-D [*Li and Valle-Levinson*, 1999] and a 3-D [*Li*, 2001] analytic tidal models with arbitrary cross-channel depth variations. We now write the three terms of equation (4) by their amplitudes and phases,

$$\begin{aligned} U &= U_1 e^{i\phi_U}, \\ \frac{\partial A}{\partial x} &= A_x e^{i\phi_{Ax}}, \\ -\frac{g}{i\sigma + \beta/h} &= B e^{i\phi_B}, \end{aligned} \quad (5)$$

in which U_1 , A_x , and B are the complex amplitude (of the semi-diurnal tidal constituent) of the longitudinal velocity, the complex amplitude of the longitudinal component of the horizontal pressure gradient, and the complex amplitude of $-g/(i\sigma + \beta/h)$; ϕ_U , ϕ_{Ax} , and ϕ_B are the (semi-diurnal tidal) phase of the longitudinal velocity, the phase of the longitudinal component of the horizontal pressure gradient, and the phase of $-g/(i\sigma + \beta/h)$, respectively. It can readily be shown that ϕ_B is

$$\phi_B = \tan^{-1} \left(\frac{\sigma}{-\beta/h} \right) = -\tan^{-1} \left(\frac{\sigma h}{\beta} \right), \quad (6)$$

and from equation (4) we have

$$\phi_U = \phi_{Ax} + \phi_B = \phi_{Ax} - \tan^{-1} \left(\frac{\sigma h}{\beta} \right). \quad (7)$$

[11] If tidal velocity can be measured across an estuary or tidal channel, the left-hand side of equation (7) is known. The friction coefficient β and the phase of the pressure

gradient ϕ_{Ax} are unknown and should be functions of the transverse position. For tidal wave problems in a narrow estuary (with width approximately a few kilometers), however, there is an important characteristic of the motion: The propagation of the wave (represented by the surface elevation) is almost one-dimensional [*Li and Valle-Levinson*, 1999], although the tidal velocity may have a strong lateral shear and thus is two-dimensional or even three-dimensional [e.g., *Li*, 2001]. In other words, the lateral variation of the surface elevation in a narrow estuary is negligible. Even for an estuary as wide as the Chesapeake Bay, the tidal elevation contours are mostly perpendicular to the axis of the channel [e.g., *Browne and Fisher*, 1988; *Spitz*, 1995] and the across-mouth variation in tidal elevation is much smaller than the tidal amplitude [*Li et al.*, 2000].

[12] We therefore assume that at tidal frequencies, the lateral variation of elevation and the lateral variation of pressure gradient are negligible. Under this assumption, equation (7) implies that ϕ_U is equal to $-\tan^{-1} \left(\frac{\sigma h}{\beta} \right)$ plus a constant ϕ_{Ax} . Since $\tan^{-1} \left(\frac{\sigma h}{\beta} \right)$ is a continuous function of h and therefore approaches zero as h approaches zero, the constant ϕ_{Ax} can be estimated from equation (7). To do this, we fit the phase ϕ_U to a polynomial of the water depth h and obtain the phase for the pressure gradient ϕ_{Ax} by requiring that h approach zero. This polynomial can be considered as a Taylor series expansion assuming that the drag coefficient only varies continuously with position or depth. The phase for the pressure gradient is the intercept. It should be noted that the procedure to obtain ϕ_{Ax} is a mathematical operation (an extrapolation to $h \rightarrow 0$) based on the fact that $\tan^{-1} \left(\frac{\sigma h}{\beta} \right)$ is a continuous function of h and does not require that h is exactly zero. The validity of this extrapolation will be examined later with an identical twin experiment. After obtaining ϕ_{Ax} , the drag coefficient is obtained from equations (7) and (2),

$$C_D = \frac{3\pi\sigma h}{8U_0 \tan(\phi_{Ax} - \phi_U)}. \quad (8)$$

The drag coefficient obtained by equation (8) is a function of ϕ_U and U_0 , which are space dependent. Since the method described above is based on the phase relationship (equation (7)) of the momentum balance (equation (4)), we call it the phase-matching method. The phase-matching method is further explained in the following section by its application to observational data obtained in the James River Estuary.

3. Drag Coefficient Estimation in James River Estuary

[13] Velocity profiles were sampled along two cross-estuary, 4-km-long transects in the lower James River (Figure 1a) throughout two spring (October 26–27) and two neap (November 2–3) tidal cycles in 1996. The profiles were obtained during 25-hour cruises with a 600-kHz Broad Band RD Instruments acoustic Doppler current profiler (ADCP). The ADCP was mounted facing downward on a small (1.2 m long) catamaran and towed at an average speed of 2.5 m/s to the starboard side of a

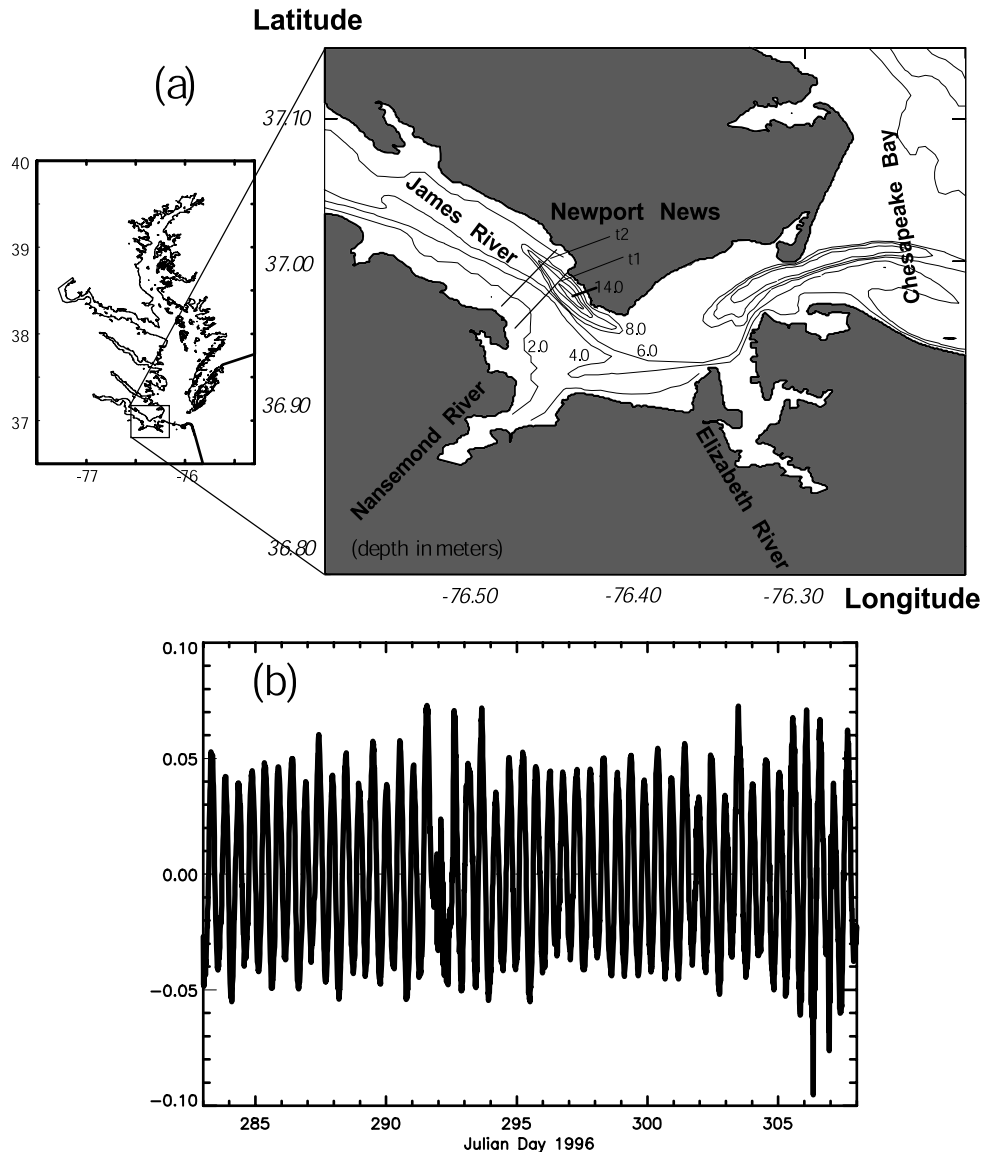


Figure 1. Study area and transverse pressure difference. (a) Study area and the two sampling transects; t1 and t2 represent the first and second transect, respectively. (b) Time series of the relative transverse variation of surface elevation in comparison to the mean elevation ($\delta a/a$), obtained from two pressure sensors across the James River in 2 months. The cross-channel difference is on the order of 5%.

25-foot boat. The ADCP recorded velocity profiles averaged over 30 s, which gave a horizontal spatial resolution of about 75 m. The bin size for vertical resolution was 0.5 m, and the closest bin to the surface was located at nearly 2 m. Compass calibration and data correction were performed following Joyce [1989]. Navigation was carried out with a differential GPS receiver. In addition to the underway sampling, which provided spatial coverage, moored digiquartz pressure sensors (SeaBird SBE 26) were deployed at both ends ($37^{\circ}0.349'N$, $76^{\circ}27.113'W$) and ($36^{\circ}58.347'N$, $76^{\circ}29.654'W$) of one transect and validated the assumption of small cross-estuary variations of surface elevation ($\sim 5\%$), relative to the tidal amplitude (Figure 1b). Time series of current velocity recorded at each point along each transect and at each depth consisted of 20 values for the spring tide cruise and 17 values for

the neap tide cruise. These time series spanned two tidal cycles and were subject to least-squares harmonic analysis on the semidiurnal and diurnal frequencies. A CTD was also used to obtain the density field across the estuary. The mean density field showed a structure typical in a partially mixed estuary (Figure 2). During the first cruise (spring tides), the density difference between the surface and bottom appeared to be slightly larger than that during the second cruise (neap tides). This was apparently caused by a larger river discharge during the first cruise than during the second cruise [Li *et al.*, 1998].

[14] After the semi-diurnal component of the vertical profiles of the horizontal velocity are obtained, it is necessary to calculate the amplitude and phase of the depth-averaged velocity at the same frequency in order to use the method of the last section to calculate the drag coefficient.

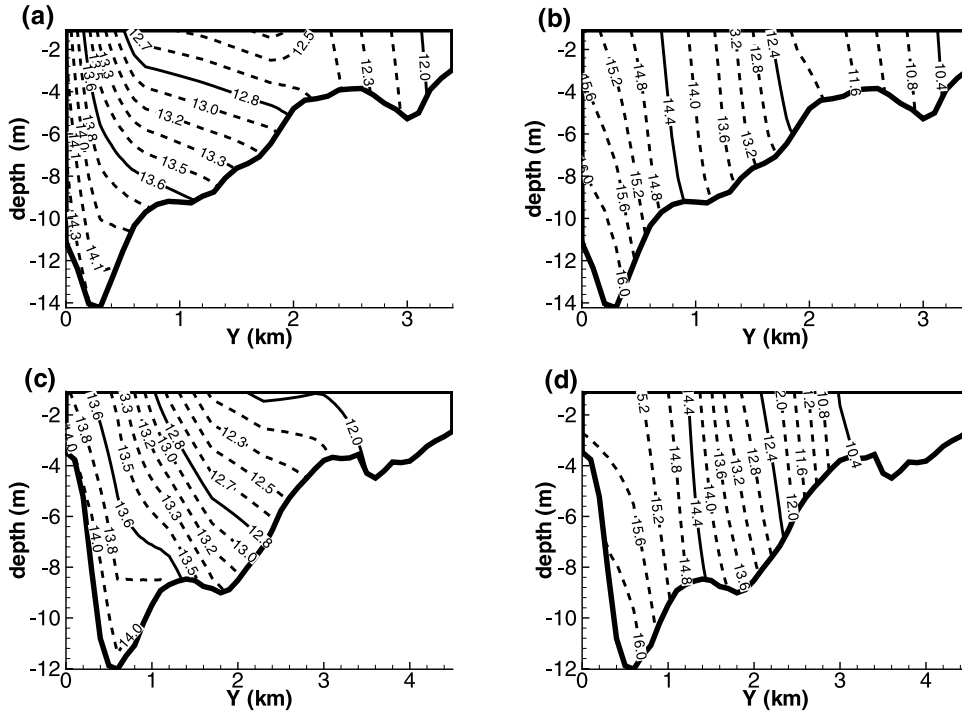


Figure 2. Mean density profiles ($\rho - 1000 \text{ kg/m}^3$). (a) Density profile for transect 1 during the first cruise (spring tide). (b) Density profile for transect 1 during the second cruise (neap tide). (c) Density profile for transect 2 during the first cruise. (d) Density profile for transect 2 during the second cruise.

Assume that the semi-diurnal tidal velocity at any given position (x, y) can be expressed as

$$u(z, t) = u_0(z) \sin(\sigma t + \phi(z)), \quad (9)$$

in which $u_0(z)$, $\phi(z)$, and z are the amplitude of the velocity, phase of the velocity, both at the semi-diurnal frequency σ , and the vertical coordinate, respectively. Note that by using equation (9), we assume that we have obtained $u_0(z)$ and $\phi(z)$ at each depth z at the given position using a harmonic analysis. Since the relation between $\phi(z)$ and $u(z, t)$, as shown by equation (9) is not linear, we cannot directly integrate $\phi(z)$ and $u_0(z)$ to get the amplitude and phase and the depth-averaged velocity. The vertically averaged velocity is defined by

$$\bar{u}(t) = \frac{1}{h} \int_{-h}^0 u(z, t) dz. \quad (10)$$

If we write the depth-averaged velocity in terms of a sine function with the same frequency, or

$$\bar{u}(t) = \bar{u}_0 \sin(\sigma t + \phi_U), \quad (11)$$

where \bar{u}_0 and ϕ_U are the amplitude and phase of the depth averaged velocity, respectively, then it can be shown, by direct derivation, that

$$\bar{u}_0 = \frac{1}{h} \sqrt{\left(\int_{-h}^0 u_0 \cos(\phi) dz \right)^2 + \left(\int_{-h}^0 u_0 \sin(\phi) dz \right)^2} \quad (12)$$

$$\phi_U = \tan^{-1} \left(\frac{\int_{-h}^0 u_0 \sin(\phi) dz}{\int_{-h}^0 u_0 \cos(\phi) dz} \right). \quad (13)$$

Obviously, if the amplitude (u_0) and phase (ϕ) of the horizontal velocity are independent of z , the amplitude (\bar{u}_0) and phase (ϕ_U) of the depth-averaged velocity will be equal to u_0 and ϕ , respectively. Note that the above reasoning involving equations (9) through (13) is purely operational. The equations can be used if the harmonic analysis to the velocity is first conducted at each depth. Alternatively, we can vertically integrate the velocity at each location and do the harmonic analysis to the depth-averaged velocity. In this case, we don't need equations (9), (12), and (13). The parameters \bar{u}_0 and ϕ_U of equation (11) are then given by the harmonic analysis. The difference between the two methods is negligible for our applications. Since we already obtained the harmonic constants at each depth [Li *et al.*, 1998], we derive these equations for the analysis of this work.

[15] As mentioned in the last section, the first step of the phase-matching method is to fit the phase of the depth-averaged velocity ϕ_U to a Taylor series expansion, assuming that the phase is a continuous function of depth. This allows us to write a polynomial of the water depth h defined by

$$\phi_U^* = a_0 + a_1 h + a_2 h^2, \quad (14)$$

where ϕ_U^* and a_i ($i = 0, 1, 2$) are the fitted phase of velocity and coefficients of the polynomial, respectively. The fitting for the ADCP data obtained in the James River Estuary in

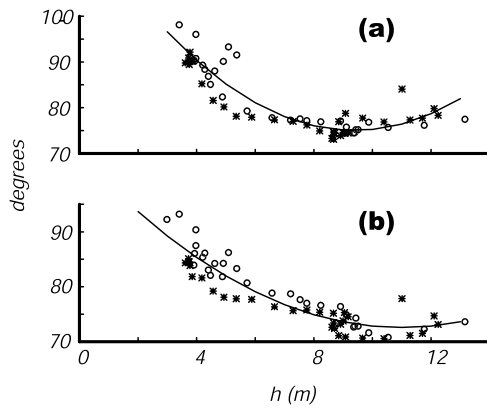


Figure 3. Depth-phase relation. The horizontal axis is the water depth in meters. The vertical axis is the phase of the longitudinal component of the semi-diurnal tidal velocity in degrees. Circles and stars are for transects 1 and 2, respectively. The solid lines show the fitted polynomial of water depth (h). (a) From data obtained during October 26–27, 1996, when the tidal elevation had a magnitude of 0.5 m (spring tides). (b) From data obtained during November 2–3, 1996, when the tidal elevation had a magnitude of 0.25 m (neap tides).

late October to early November of 1996 is shown in Figure 3. The coefficients a_0 , a_1 , and a_2 for the spring tides (October 26–27) are 121.59 (degree), -9.93 (degree/M), and 0.53 (degree/M²), respectively. For the neap tides (November 2–3), these coefficients are -21.72 (degree), -11.48 (degree/M), and 0.52 (degree/M²), respectively. The RMS of the fitting is about 5° , which is equivalent to 10 min for semi-diurnal tide. Since our typical phase lag can be 20 – 30° (i.e., up to 1 hour), this is relatively small. The estimated phase of the pressure gradient is $\phi_{Ax} = a_0$. The drag coefficient is then calculated with equation (8), the formula obtained from the phase-matching method. Figure 4 shows the drag coefficient for both the spring tides (October 26–27, 1996) and the neap tides (November 2–3, 1996) and fitted quadratic functions of the water depth h . The standard deviation of the fitting for the drag coefficient is about 5×10^{-4} .

[16] The classical “standard” value of the bottom drag coefficient is 0.0025 [Proudman, 1953], although the actual value is case dependent and can be quite variable. The present results show that the estimated drag coefficient has the correct order of magnitude: C_D varies from 1.2×10^{-3} to 6.9×10^{-3} with a transverse mean value of 2.2×10^{-3} for the spring tides and 2.3×10^{-3} for the neap tides (Figure 4). The spring-neap variation of the transverse mean is thus not obvious during this time period. However, some cross-channel differences between the spring and neap are observable. The drag coefficient in shallow waters (h less than 9 m) appear to have larger values in neap than in spring while the drag coefficient in deep waters (h larger than 9 m) appear to have smaller values in neap than in spring (Figure 4). This difference is about the same order of the standard error mentioned above (5×10^{-4}). The cause of the difference, if significant, is not known. More observations and analysis will be required to establish the statistical significance of this

difference in shallow and deep waters from spring to neap and to determine the physics behind it.

[17] Secondly, the drag coefficient is a function of the water depth with the largest values on the shoals. The drag coefficient reaches its minimum also at around $h = 9$ m and increases slightly in the deep water from 12 to 14 m. Overall, the result is consistent with those of Ullman and Wilson [1998] and Spitz and Klinck [1998] such that in shallower waters, C_D is larger. The overall pattern of the C_D - h relationship fits the relationship between the drag coefficient and the ratio between water depth and the bottom roughness under no stratification [Moffeld, 1988]: The larger the ratio between water depth and the bottom roughness, the smaller the drag coefficient. The exceptions in the deep water might indicate that the bottom roughness is not uniform across the transect. We may also interpret the minimum drag coefficient at the 9-m water with the following reasoning. The two cross sections have 9-m plateaus bounded by a narrow trench on the left-hand side (facing downstream direction) shown in the figures (up to 12–14 m deep). Over the plateaus, the depth-averaged velocity amplitude is the maximum [Li and Valle-Levinson, 1999]. Although there is a slight increase of depth-averaged velocity over the deep trench, the increase is quite small (almost constant). The phase over the trench is also constant or even slightly reversed. This is most likely a result of the increased side boundary friction as the trench is on the northern boundary but the model does not include the lateral friction. Nor could we include the lateral friction if we were still going to solve it analytically as has been done. Indeed, the drag coefficient is larger near the banks than in the center. The minimum drag coefficient near 9 m therefore appears to be caused by lateral friction of the side boundaries.

[18] It is important to note that in the present model, as in the models of Ullman and Wilson [1998] and Spitz and Klinck [1998], stratification was not included. This may have influenced the “apparent” drag coefficient calculated by the barotropic models used in these (including the present) studies. Indeed, these two-dimensional adjoint variational barotropic numerical models yielded contradictory results.

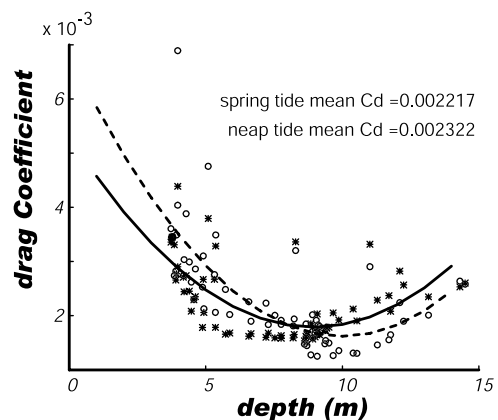


Figure 4. Drag coefficient as a function of the water depth. Circles and stars are for the spring tides and neap tides, respectively. The solid line and the dashed line show the fitted polynomial of water depth (h) during the spring and neap tides, respectively.

The adjoint variational method of *Spitz* [1995] and *Spitz and Klinck* [1998] applied to the Chesapeake Bay showed that the drag coefficient was larger during neap tides than during spring tides. In contrast, *Ullman and Wilson* [1998] showed larger drag coefficient values in the Hudson River during spring tides than during neap tides. In this study, we have found a third possibility: The transverse mean drag coefficient did not change in the James River Estuary from spring tides to neap tides during our observations. However, as discussed above, our results indicate a larger drag coefficient in neap tides than in spring tides in shallow waters but a smaller drag coefficient in neap tides than in spring tides in deep waters (with 9 m as the division between shallow and deep waters). The difference between spring and neap tides is comparable to the standard error (5×10^{-4}) of the estimated drag coefficient. Therefore, its statistical significance is not well established, from this data set. A physical explanation of the conflicting results can be made based on a consideration about the effect of stratification and tidal mixing. Increased tidal mixing can increase drag coefficient, just as *Ullman and Wilson* [1998] argued. However, increased river discharge can limit tidal mixing, thus lowering the drag coefficient. During our studies, the tidal amplitude reduced by half (from 0.5 m to 0.25 m) from spring tides to neap tides. Smaller tidal amplitude should result in weaker tidal mixing [*Simpson and Hunter*, 1974]. At the same time, the river discharge reduced by about half as well (from 132 to 56 m³/s) [*Li et al.*, 1998]. As a result, during spring tide, the stratification was stronger than that during neap tide (Figure 2). Therefore, averaged across the channel, the increased tidal motion during spring tide apparently did not cause a significantly increased tidal mixing because of increased river discharge. Our result of unchanged transverse mean drag coefficient from spring to neap can be explained by the nearly canceling effect of the two when a weaker tidal forcing of neap tides coincided with a weaker river discharge or a stronger tidal forcing coincided with a larger river discharge that in turn limited the tidal mixing. According to experimental results [*Linden and Simpson*, 1988], observations in estuaries [*Peters*, 1997], an empirical relationship [*Bowden*, 1967], and a Taylor series expansion [*Li et al.*, 1998], it can be shown that, to first order, tidal mixing is proportional to tidal amplitude and stratification is proportional to river discharge. Consequently, our result can be explained at least qualitatively since both the tidal amplitude and river discharge decreased by about half from spring tides to neap tides.

4. Validation of the Phase-Matching Method

[19] In section 2, we have developed a method to estimate the bottom drag coefficient as a function of water depth. In section 3, we have applied this method to some ADCP data obtained in the James River Estuary. In this section, we will further test the method by some “identical twin experiments” (ITEs). The first step of the ITE is to solve an analytic model with a given spatial distribution of bottom drag coefficient in a rectangular domain with variable cross-channel depth variation. The second step uses the velocity field obtained from the analytic model as hypothetical observations and applies the phase-matching method to calculate the drag coefficient. Note that the second step

uses the empirical method proposed above and does not involve the model. By comparing the drag coefficient obtained in the second step to that specified in the first step, the validity of the phase-matching method can be tested. We have conducted the ITEs with two different approaches for the second step for comparison: One uses the model velocity as is and the other uses the velocity field plus a random noise, to recover the drag coefficient. As one more step beyond the ITEs for further examination of the model performance, we will then apply the drag coefficient estimated from the phase-matching method as a function of cross-channel position in the analytic model to calculate the velocity field and compare with the observations.

4.1. First Step: Solving an Analytic Model

[20] The model is based on an earlier model of *Li and Valle-Levinson* [1999], which was verified by comparing to an exact solution and by a momentum balance calculation. Here we extend the solution to allow a variable drag coefficient in the transverse direction. The most important aspect of the model is that it is based on the assumption that the lateral variation of the elevation in a narrow estuary is small, a characteristic we have discussed in section 2. In the following, we outline the method and the solution. The depth-averaged momentum and continuity equations, correct to the first order ($\mathcal{O}(a/h)$, a ratio of tidal amplitude and mean depth) are

$$\begin{aligned}\frac{\partial u}{\partial t} &= -g \frac{\partial \zeta}{\partial x} - \frac{\beta}{h} u, \\ \frac{\partial v}{\partial t} &= -g \frac{\partial \zeta}{\partial y} - \frac{\beta}{h} v, \\ \frac{\partial \zeta}{\partial t} + h \frac{\partial u}{\partial x} + \frac{\partial hv}{\partial y} &= 0.\end{aligned}\quad (15)$$

[21] The depth function is assumed to be a function of the across-estuary position,

$$h = h(y). \quad (16)$$

[22] For a single frequency co-oscillating tide, the solution can be expressed as

$$u = Ue^{i\sigma t}, \quad v = Ve^{i\sigma t}, \quad \zeta = Ae^{i\sigma t}, \quad (17)$$

where σ , i , U , V , and A are the angular frequency of the tide, the unit imaginary number $\sqrt{-1}$, the complex amplitude of the longitudinal velocity, the complex amplitude of the transverse velocity, and the complex amplitude of the tidal elevation, respectively.

[23] Substituting equations (17) into equations (15) yields

$$\begin{aligned}i\sigma U &= -g \frac{\partial A}{\partial x} - \frac{\beta}{h} U, \\ i\sigma V &= -g \frac{\partial A}{\partial y} - \frac{\beta}{h} V, \\ i\sigma A + h \frac{\partial U}{\partial x} + \partial h V \partial y &= 0.\end{aligned}\quad (18)$$

[24] For a co-oscillating tide problem, the tidal amplitude at the estuary mouth is usually known. The longitudinal

velocity at the head ($x = L$, a solid boundary) vanishes. For simplicity, we specify that the side boundaries are parallel to each other and the y axis is thus perpendicular to the side boundaries. The transverse velocity at the side boundaries ($0, D$) must therefore be zero. Hence the boundary conditions are

$$A \Big|_{x=0} = a, \quad \frac{\partial A}{\partial x} \Big|_{x=L} = 0, \quad V \Big|_{y=0,D} = 0. \quad (19)$$

[25] The first equation of (18) yields

$$U = -\frac{g}{i\sigma + \beta/h} \frac{\partial A}{\partial x} \quad (20)$$

$$\frac{\partial U}{\partial x} = -\frac{g}{i\sigma + \beta/h} \frac{\partial^2 A}{\partial x^2}. \quad (21)$$

[26] *Li* [1996] has shown that based on a perturbation solution, the lateral variation of tidal elevation in an estuary or tidal river of a few kilometers wide is very small compared to that of the longitudinal variation. We therefore assume that the lateral variation of elevation is negligible in the x -momentum and the continuity equations. The complex amplitude of the tidal elevation is therefore taken to be approximately independent of y , which leads to a dramatic simplification of the solution.

[27] Multiplying equation (29) by h and then integrating the product across the estuary from $y = 0$ to $y = D$ (the width of the estuary) yields

$$\int_0^D h \frac{\partial U}{\partial x} dy = -\int_0^D \frac{gh}{i\sigma + \beta/h} \frac{\partial^2 A}{\partial x^2} dy \approx \mathcal{F} \frac{\partial^2 A}{\partial x^2}, \quad (22)$$

where

$$\mathcal{F} = -\int_0^D \frac{gh}{i\sigma + \beta/h} dy, \quad (23)$$

in which β can be an arbitrary function of y .

[28] Note that we have neglected the lateral variation of $\partial^2 A / \partial x^2$ in obtaining equation (22) due to the assumption we made. The error of the approximation of equation (22) is $\mathcal{F} \partial^2 |\Delta A| / \partial x^2$, where ΔA is the lateral variation of A . The relative error is therefore $|\partial^2 \Delta A / \partial x^2| / |\partial^2 A / \partial x^2| \sim |\Delta A| / |A|$. As shown by Figure 1b, the observed magnitude of $|\Delta A| / |A|$ in the James River Estuary is about 5%. The error of approximation of equation (22) is therefore about 5% for the James River Estuary. Integrating the continuity equations (18) across the estuary and applying the lateral boundary conditions in equations (19) yields

$$i\sigma AB + \mathcal{F} \frac{\partial^2 A}{\partial x^2} = 0. \quad (24)$$

Again, we have used the assumption, that A is laterally independent, in obtaining equation (24). Equation (24) has a solution satisfying the boundary conditions (19) for A ,

$$A = a \frac{\cos(\omega(x-L))}{\cos(\omega L)}, \quad (25)$$

in which

$$\omega^2 = \frac{i\sigma B}{\mathcal{F}}. \quad (26)$$

[29] Consequently, we have, by virtue of equations (25) and (20), the solutions for U and the along-channel gradients of A and U as follows:

$$U = \frac{g}{i\sigma + \beta/h} \frac{a\omega}{\cos(\omega L)} \sin(\omega(x-L)), \quad (27)$$

$$\frac{dA}{dx} = -\frac{a\omega}{\cos(\omega L)} \sin(\omega(x-L)), \quad (28)$$

$$\frac{\partial U}{\partial x} = \frac{g}{i\sigma + \beta/h} \frac{a\omega^2}{\cos(\omega(x-L))} = \frac{g\omega^2}{i\sigma + \beta/h} A. \quad (29)$$

[30] With a straightforward derivation, A , U , and their derivatives can be obtained in terms of their real and imaginary parts [*Li and Valle-Levinson*, 1999]. Alternatively, we can use some commonly used computer languages, such as MATLAB and IDL, that allow complex variables and functions, for direct calculations without separating the real and imaginary parts. The present model is programmed in MATLAB. Now both A and U are solved and expressed in simple forms for any depth function $h(y)$. This solution is identical to the one presented by *Li and Valle-Levinson* [1999], except that here, C_D or β is allowed to be a function of y . Evidently, the lateral dependence of U is dictated by the forms of $C_D(y)$ and $h(y)$ as shown by equation (27). For a constant h and a constant C_D , the solution is the same as those of previous theories [e.g., *Ippen and Harleman*, 1961; *Officer*, 1976]. Substituting equation (29) into the third equation of (18), it yields

$$i\sigma A + \frac{gh\omega^2}{i\sigma + \beta/h} A + \frac{\partial hV}{\partial y} = 0, \quad (30)$$

which can be used to solve V by integration with respect to y ,

$$V = -\frac{1}{h} \left(i\sigma y + \int_0^y \frac{gh\omega^2}{i\sigma + \beta/h} dy \right) A. \quad (31)$$

[31] It follows from the second equation of (18) and (31) that

$$\begin{aligned} \frac{\partial A}{\partial y} &= -\frac{1}{g} (i\sigma + \beta/h) V \\ &= \frac{i\sigma + \beta/h}{gh} \left(i\sigma y + \omega^2 \int_0^y \frac{gh}{i\sigma + \beta/h} dy \right) A, \end{aligned} \quad (32)$$

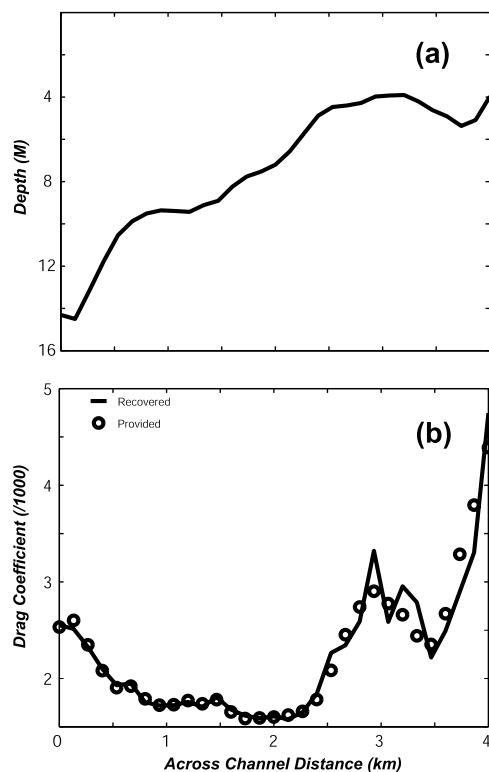


Figure 5. Identical Twin Experiment (1), results for the first transect. (a) Depth distribution across the channel. (b) Comparison between the given and inferred drag coefficients. The circles are the given values, while the line is calculated.

from which the magnitude of $\partial A/\partial y$ can be calculated and used to check the assumption that A is almost laterally uniform, which has been discussed by *Li and Valle-Levinson* [1999].

4.2. Second Step: Recovering Drag Coefficient

[32] Two ITEs are conducted. The observed cross-channel depth distributions along the two transects of the James River (Figures 5a and 6a) are used. The drag coefficient as a function of cross-channel distance is given by the results of section 3. The length and width of the models are 70 km and 4 km, respectively. In all experiments, tidal amplitude at the open boundary is chosen to be 1 m. The analytic solution is calculated for each ITE model to obtain the velocity field. The velocity field along a transverse line at different distances from the mouth is then used as hypothetical observational data, and the phase-matching method is applied. In our presentation, we only demonstrate the results from a cross section at 10 km inside the mouth, typical of all results from different cross sections. When no noise is added to the velocity field, the drag coefficient is accurately recovered in each case. It should be emphasized that the accurate recovery of the drag coefficient demonstrates that the extrapolation at $h \rightarrow 0$ that leads to equation (8) is correct. It can be shown that by altering equation (8) even slightly, the accurate recovery will not be possible.

[33] Next, we add a random error to the velocity field from each of the two models. The random function has a zero mean defined by the MATLAB function. The magnitude of the random error velocity is between -0.10 m/s and 0.10 m/s, with the maximum model produced velocity of about 0.80 m/s. Figures 5b and 6b show the comparison between the given drag coefficients used in producing the hypothetical observational (i.e., the model) velocity and the recovered drag coefficients from equation (8). In each case, with only the depth distribution across the channel and the velocity field, we are able to infer the drag coefficient distribution that is needed to produce the velocity field. The inferred and given drag coefficients are consistent in each test.

[34] Note that the phase-matching method is independent of the analytic model; that is, in implementing the second step, the dynamical equations are not used and only the equations of section 2 (particularly equation (8)) are used. From these ITE results, we conclude that the phase-matching method does reflect the tidal dynamics in idealized occasions (no observational errors). Even with a moderate random error of velocity field, which is always present in real observations, the method can still successfully recover the drag coefficients.

[35] It should also be noted that the phase-matching method presented here is applicable to data from a cross section of the tidal channel. By applying the method to

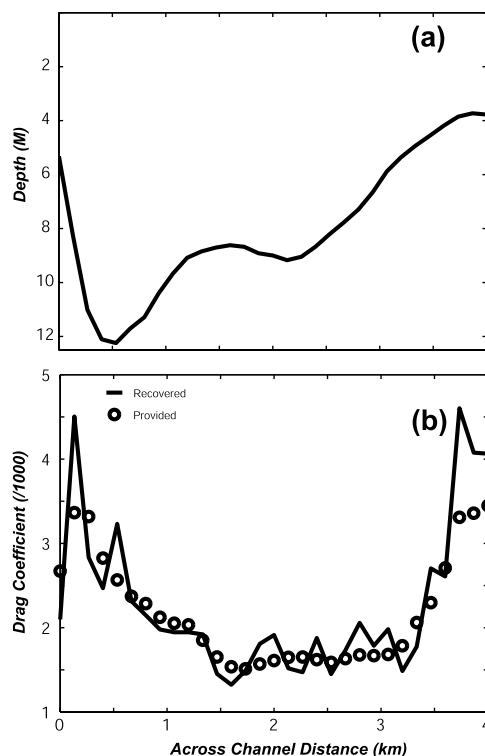


Figure 6. Identical Twin Experiment (2), results for the second transect. (a) Depth distribution across the channel. (b) Comparison between the given and inferred drag coefficients. The circles are the given values, while the line is calculated.

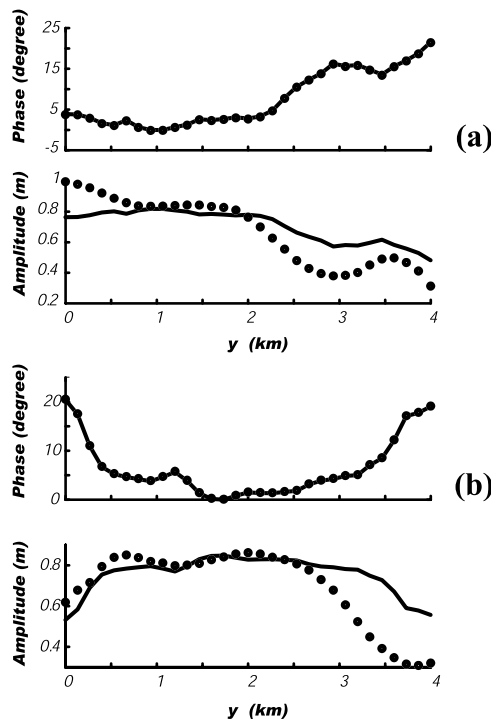


Figure 7. Comparison between model and observations. The model results are obtained by applying the drag coefficient values calculated from the phase-matching method to the analytical model of section 4. (a) First transect. (b) Second transect. The model results are denoted by the circles, and the observations are shown by the lines.

different cross sections along the channel, we can obtain a two-dimensional distribution of the bottom drag coefficient just as a two-dimensional adjoint variational model would. To conduct concurrent observations along multiple transects, however, is not generally practiced because of logistic reasons and cost of operations.

4.3. Comparison of Calculated and Observed Flow Fields

[36] By applying the drag coefficient values calculated from section 3 to the two-dimensional model of section 4.1, we have calculated the tidal flow field for comparison with the observations. The comparison is shown in Figure 7. Figures 7a and 7b are for the two transects, respectively. They show the cross-channel distributions of the phase and amplitude of the major (M_2) tidal component of the depth-averaged velocity. Apparently, the model phase matches that of the observations, as required by the method. The distribution of the velocity amplitude reproduces the general characteristics of the observed velocity amplitude, but it has some relatively large errors at a number of places, especially near the banks of the estuary. The best performance of the model appears to be in the center of the channel. This supports the idea that the lateral friction, which is missing in the analytical model, may be important and contributes to the effective bottom drag coefficient at near the banks. Although the analytical

model is linear and quite simplified and the errors are large at places, the comparison nevertheless demonstrates that the drag coefficient values obtained from the phase-matching method are generally valid.

5. Additional Discussion and Summary

[37] In this paper, we have developed a phase-matching method to estimate the bottom drag coefficient for the depth-averaged, semi-diurnal and barotropic motion. It is suitable for tidally dominated estuaries with narrow width (much smaller than the Rossby deformation radius) and shallow water depth. It is applicable to the velocity measurement along a transverse section for at least one tidal cycle. The technique is introduced with the assumption that the lateral variation of elevation, and thus that of the longitudinal pressure gradient, is negligible. The calculation involves a few steps. First, the observed horizontal velocity components are analyzed by harmonic decomposition so that the amplitude and phase of the velocity at the major tidal frequency are obtained. The phase of the longitudinal velocity is then fitted to a quadratic function of the water depth to obtain the phase of the pressure gradient. The drag coefficient, as a function of the transverse position, is then calculated from the phase relationship of the longitudinal momentum equation. The application of this method to the ADCP data obtained in the James River Estuary yields a drag coefficient distribution across the channel with a mean value of $\sim 2.2 \times 10^{-3}$. The drag coefficient is larger in the shallow water than in the deep water. The drag coefficient is larger near the banks, indicating an effect of increased lateral friction. Since lateral friction is not included in the model, the lateral friction is “folded” into the bottom friction in effect. The variation of the transverse mean drag coefficient between the spring and neap tides is not obvious, a result that can be attributed to the canceling effect of a weaker mixing coinciding with a weaker river discharge during the neap tides.

[38] To validate the phase-matching method, we have designed and conducted two ITEs. The ITEs involve two steps. The first step solves an analytic model with a given spatial distribution of bottom drag coefficient in a rectangular domain. The second step uses the velocity field obtained from the analytic model as hypothetical observational data and applies the phase-matching method to recover the drag coefficient. The tests show that the phase-matching method can correctly recover the drag coefficient. By using the drag coefficient estimated from the phase-matching method and applying the two-dimensional analytic model, we have demonstrated a general agreement of the flow field between the model and the observations.

[39] The phase-matching method presented here is based on the linearized momentum equation. As demonstrated by, for example, *Parker* [1984], nonlinear effect can contribute to errors as much as 17%. An extended discussion on the nonlinear effect may be accomplished by using a numerical model that includes all the nonlinear terms in the momentum and continuity equations. The present method is obviously limited to only linear problems because of the limit of an analytical approach. We expect that, for example, if a spatial variability of drag coefficient is much larger than

10% (as is the case of the present problem, where the drag coefficient ranges from 1.2×10^{-3} to 6.9×10^{-3}), the present model would provide the correct characteristics of spatial distribution unless the nonlinear effect is too strong to be negligible.

[40] The application of the phase-matching method in this paper has used the ADCP data from a moving platform. Data from an ADCP on a moving platform have larger errors than those from a bottom-mounted ADCP. However, in most cases a moving platform involving only a small vessel is convenient and cost effective. Many bottom-mounted ADCPs would be required to resolve the cross-channel variation of velocity field comparable to that from a vessel-based moving ADCP. If enough bottom-mounted ADCPs are used in a cross section of a tidally dominated channel, the phase-matching method proposed here will also be applicable and the results should have even less error.

[41] **Acknowledgments.** This project has been supported by the U.S. National Science Foundation (NSF Project OCE-9529806, OCE-9530394, and OCE-9530395), Georgia Sea Grant (RR746-007/7512067), South Carolina Sea Grant (NOAA NA960PO113), and Georgia DNR (RR100-279-9262764). Dozens of faculty members, staff, and students from CCPO, State University of New York, and University of Delaware participated in the field work, and their help was invaluable. We appreciate the thorough and constructive reviews of two anonymous reviewers, which were helpful in the improvement of the paper.

References

- Bang, B. (1994), Inverse estimation of horizontal pressure gradients and vertical eddy viscosity profiles in shallow waters, Ph.D. dissertation, 154 pp., School of Mar. Sci., Coll. of William and Mary, Williamsburg, Va.
- Bowden, K. F. (1967), Stability effects on turbulent mixing in tidal currents, *Phys. Fluids*, 10, Suppl., S278–S280.
- Bowden, K. F., and L. A. Fairbairn (1952), A determination of the friction forces in a tidal current, *Proc. R. Soc. London, Ser. A*, 214, 371–392.
- Browne, D. R., and C. W. Fisher (1988), Tide and tidal currents in the Chesapeake Bay, *NOAA Tech. Rep., NOS OMA 3*, 84 pp.
- Clarke, A. J. (1990), Application of a frictional channel flow theory to flow in the Prince of Wales Channel, Torres Strait, *J. Phys. Oceanogr.*, 20, 890–899.
- Friedrichs, C. T., and L. D. Wright (1997), Sensitivity of bottom stress and bottom roughness estimates to density stratification, Eckernförde Bay, *J. Geophys. Res.*, 102, 5721–5732.
- Godfrey, J. S. (1980), A numerical model of the James River Estuary, Virginia, U.S.A., *Estuarine Coastal Mar. Sci.*, 11, 295–310.
- Hansen, D. V., and M. Rattray Jr. (1965), Gravitational circulation in straits and estuaries, *J. Mar. Res.*, 23, 104–122.
- Huntley, D. A., R. J. Nicholls, C. Liu, and K. R. Dyer (1994), Measurements of the semi-diurnal drag coefficient over sand waves, *Cont. Shelf Res.*, 14, 437–456.
- Ippen, A. T., and D. R. F. Harleman (1961), One-dimensional analysis of salinity intrusion in estuaries, report, 52 pp., U.S. Army Corps of Eng., Washington, D. C.
- Joyce, T. M. (1989), On in situ calibration of shipboard ADCPs, *J. Atmos. Oceanic Technol.*, 6(1), 169–172.
- Kuo, A. Y., J. Shen, and J. M. Hamrick (1996), Effect of acceleration on bottom shear stress in tidal estuaries, *J. Waterw. Port Coastal Ocean Eng.*, 122, 75–83.
- Lardner, R. W., and S. K. Das (1994), Optimal estimation of eddy viscosity for a quasi-three-dimensional numerical tidal and storm surge model, *Int. J. Num. Methods Fluids*, 18, 295–312.
- Lardner, R. W., and Y. Song (1995), Optimal estimation of eddy viscosity and friction coefficients for a quasi-three-dimensional numerical tidal model, *Atmos. Ocean*, 33, 581–611.
- LeBlond, P. H. (1978), On tidal propagation in shallow rivers, *J. Geophys. Res.*, 83, 4717–4721.
- Li, C. (1996), Tidally induced residual circulation in estuaries with cross channel bathymetry, Ph.D. dissertation, 242 pp., Univ. of Conn., Storrs, Conn.
- Li, C. (2001), 3D Analytic model for testing numerical tidal models, *J. Hydraul. Eng.*, 127(9), 709–717.
- Li, C., and A. Valle-Levinson (1999), A two-dimensional analytic tidal model for a narrow estuary of arbitrary lateral depth variation: The intratidal motion, *J. Geophys. Res.*, 104, 23,525–23,543.
- Li, C., A. Valle-Levinson, K.-C. Wong, and K. M. M. Lwiza (1998), Separating baroclinic flow from tidally induced flow in estuaries, *J. Geophys. Res.*, 103, 10,405–10,417.
- Li, C., A. Valle-Levinson, L. P. Atkinson, and T. C. Royer (2000), Inference of tidal elevation in shallow water using a vessel-towed ADCP, *J. Geophys. Res.*, 105, 26,225–26,236.
- Linden, P. F., and J. E. Simpson (1988), Modulated mixing and frontalgenesis in shallow seas and estuaries, *Cont. Shelf Res.*, 8, 1107–1127.
- Lueck, R. G., and Y. Y. Lu (1997), The logarithmic layer in a tidal channel, *Cont. Shelf Res.*, 17, 1785–1801.
- Mofjeld, H. O. (1988), Depth dependence of bottom stress and quadratic drag coefficient for barotropic pressure-driven currents, *J. Phys. Oceanogr.*, 18, 1658–1669.
- Officer, C. B. (1976), *Physical Oceanography of Estuaries*, 465 pp., John Wiley, New York.
- Panchang, V. G., and J. E. Richardson (1993), Inverse adjoint variational estimation of eddy viscosity for coastal flow models, *J. Hydraul. Eng.*, 119, 506–524.
- Parker, B. B. (1984), Frictional effects on the tidal dynamics of shallow estuary, Ph.D. dissertation, 291 pp., Johns Hopkins Univ., Baltimore, Md.
- Parker, B. B. (1991), The relative importance of the various nonlinear mechanisms in a wide range of tidal interactions (review), in *Tidal Hydrodynamics*, edited by B. B. Parker, pp. 237–268, John Wiley, New York.
- Peters, H. (1997), Observations of stratified turbulent mixing in an estuary: Neap to spring variations during high river flow, *Estuarine Coastal Shelf Sci.*, 45, 69–88.
- Proudman, J. (1953), *Dynamical Oceanography*, 409 pp., Methuen, New York.
- Simpson, J. H., and J. R. Hunter (1974), Fronts in Irish Sea, *Nature*, 250, 404–406.
- Spitz, Y. H. (1995), A feasibility study of dynamical assimilation of tide gauge data in the Chesapeake Bay, Ph.D. dissertation, 167 pp., Old Dominion Univ., Norfolk, Va.
- Spitz, Y. H., and J. M. Klinck (1998), Estimate of bottom and surface stress during a spring-neap tide cycle by dynamical assimilation of tide gauge observations in the Chesapeake Bay, *J. Geophys. Res.*, 103, 12,761–12,782.
- Ten Brummelhuis, P. G. J., A. W. Heemink, and H. F. P. Van De Boogaard (1993), Identification of shallow sea models, *Int. J. Num. Methods Fluids*, 17, 637–665.
- Thacker, W. C. (1988), Fitting models to inadequate data by enforcing spatial and temporal smoothness, *J. Geophys. Res.*, 93, 10,655–10,665.
- Thacker, W. C. (1989), The role of the Hessian Matrix in fitting models to measurements, *J. Geophys. Res.*, 94, 6177–6196.
- Thacker, W. C., and R. B. Long (1988), Fitting dynamics to data, *J. Geophys. Res.*, 93, 1227–1240.
- Ullman, D., and R. E. Wilson (1998), Model parameter estimation from data assimilation modeling: Temporal and spatial variability of the bottom drag coefficient, *J. Geophys. Res.*, 103, 5531–5549.
- Valle-Levinson, A., C. Li, T. C. Royer, and L. P. Atkinson (1998), Flow patterns at the Chesapeake Bay entrance, *Cont. Shelf Res.*, 18, 1157–1177.
- Wang, X. H., and P. D. Craig (1993), An analytic model of tidal circulation in a narrow estuary, *J. Mar. Res.*, 51, 447–465.
- Wilkinson, R. H. (1986), Variation of roughness length of a mobile sand bed in a tidal flow, *Geo Mar. Lett.*, 5, 231–239.

L. P. Atkinson and A. Valle-Levinson, Center for Coastal Physical Oceanography, Old Dominion University, Norfolk, VA 23508, USA. (larry@ccpo.odu.edu; arnoldo@ccpo.odu.edu)

C. Li, Skidaway Institute of Oceanography, 10 Ocean Science Circle, Savannah, GA 31411, USA. (chunyan@skio.peachnet.edu)

K. M. M. Lwiza, Marine Sciences Research Center, State University of New York, Stony Brook, NY 11794, USA. (klwiza@notes.cc.sunysb.edu)

K. C. Wong, College of Marine Studies, University of Delaware, Newark, DE 19716, USA. (kuo@newark.cms.udel.edu)